Published OnlineFirst July 9, 2012; DOI: 10.1158/0008-5472.CAN-12-0136

Cancer Research

Global Quantitative Phosphoproteome Analysis of Human Tumor Xenografts Treated with a CD44 Antagonist

Stefan Weigand[1], Frank Herting[1], Daniela Maisel[1], Adam Nopora[1], Edgar Voss[1], Christoph Schaab[2,3], Martin Klammer[2], and Andreas Tebbe[2]

Abstract

The cell surface glycoprotein CD44 plays an important role in the development and progression of various tumor types. RG7356 is a humanized antibody targeting the constant region of CD44 that shows antitumor efficacy in mice implanted with CD44-expressing tumors such as MDA-MB-231 breast cancer cells. CD44 receptor seems to function as the main receptor for hyaluronic acid and osteopontin, serving as coreceptor for growth factor pathways like cMet, EGFR, HER-2, and VEGFR and by cytoskeletal modulation via ERM and Rho kinase signaling. To assess the direct impact of RG7356 binding to the CD44 receptor, a global mass spectrometry–based phosphoproteomics approach was applied to freshly isolated MDA-MB-231 tumor xenografts. Results from a global phosphoproteomics screen were further corroborated by Western blot and ELISA analyses of tumor lysates from CD44-expressing tumors. Short-term treatment of tumor-bearing mice with RG7356 resulted in modifications of the MAPK pathway in the responsive model, although no effects on downstream phosphorylation were observed in a nonresponsive xenograft model. Taken together, our approach augments the value of other high throughput techniques to identify biomarkers for clinical development of targeted agents. *Cancer Res; 72(17); 4329–39. ©2012 AACR.*

Introduction

The cell adhesion molecule CD44 is a transmembrane glycoprotein overexpressed and linked to bad prognosis in a number of tumor entities such as breast (1–3) and pancreatic cancer (4, 5), hepatocellular carcinoma (6) and hematologic malignancies (7). CD44 receptor varies in size and function owing to *N*- and *O*-glycosylation and alternative splicing, which affects predominantly the extracellular domain of the protein. Despite not being a direct signaling molecule, CD44 is said to be involved in a variety of functions that promote tumor development, progression and metastasis (8). CD44 acts as the main receptor for hyaluronic acid and osteopontin, participates in signal transduction processes by establishing specific transmembrane complexes with growth factor receptors such as cMet, EGFR, HER2, and VEGF-R and by organizing signaling cascades through association with the cytoskeleton via ERM signaling and Rho kinase pathways (9, 10). Most evidence of the functional role of CD44 has been obtained from cell culture experiments with antibodies against all CD44 molecules or specific splice variants, activation of the receptor by its natural ligands HA (11) or osteopontin (12), or by gain or loss of function experiments *in vivo* (9). Herein we describe the direct effect of RG7356, a novel humanized anti-CD44 monoclonal antibody directed against the constant region of CD44, on human tumor cells in xenotransplanted mice by a global mass spectrometry-based phosphoproteomics approach. This study revealed short-term effects of CD44-targeting on MAPK pathway that were further confirmed by alternative methods (Western blot and ELISA). In a tumor model that was nonresponsive to RG7356 treatment, this pathway remained unchanged.

Materials and Methods

Cell lines and culture

MDA-MB-231 were grown in RPMI1640 supplemented with 2 mmol/L L-glutamine and 10% heat-inactivated FBS. PL-45 were grown in Dulbecco's Modified Eagle's Medium supplemented with 2 mmol/L L-glutamine and 10% heat-inactivated FBS. All media and supplements were purchased from PAN Biotech (Aidenbach).

For the xenograft phosphoproteomics study heavily SILAC labeled MDA-MB-231cells served as the shared reference. Therefore, cells were grown as described earlier in RPMI1640 supplemented with 2 mmol/L L-glutamine and 10% heat-inactivated FBS medium lacking arginine and lysine and supplement with dialyzed serum and the corresponding concentrations of the heavy isotopic forms L-arginine-U-$^{13}C_6$ $^{15}N_4$ and L-lysine-U-$^{13}C_6$ $^{15}N^2$. After full label incorporation, cells were lyzed in 8 M urea lysis buffer containing 50 mmol/L Tris pH 8.2, 10 mmol/L sodium pyrophosphate, 5 mmol/L EDTA,

Authors' Affiliations: [1]Discovery Oncology, Pharma Research and Early Development, Roche Diagnostics GmbH, Penzberg; [2]Evotec AG; and [3]Max Planck Institute of Biochemistry, Martinsried, Germany

Note: Supplementary data for this article are available at Cancer Research Online (http://cancerres.aacrjournals.org/)

Corresponding Author: Stefan Weigand, Roche Diagnostics GmbH, Nonnenwald 2, 82377 Penzberg, Germany. Phone: 49-8856-60-4749; Fax: 49-8856-6079-4749; Email: Stefan.weigand@roche.com

doi: 10.1158/0008-5472.CAN-12-0136

Published OnlineFirst July 9, 2012; DOI: 10.1158/0008-5472.CAN-12-0136

5 mmol/L EGTA, 10 mmol/L sodium fluoride, 10 mmol/L β-glycerophosphat, 10 mmol/L sodium orthovanadate, HALT phosphatase inhibitor cocktail (Pierce, 1:100, v/v) and Complete Protease Inhibitor Cocktail Tablets (Roche). The protein concentration was determined by Bradford and the suspension was stored at −80°C until use.

Antibodies and chemicals

ERK1/2 (137F5), p-ERK1/2 (Thr202/Tyr204; D13.14.4E), p-GSK3β (Ser9) (5B3), eIF4E (#9742), p-eIF4E (Ser209; #9741), STAT3α/β (#9132), MEK1/2 (#9122), and p-MEK1/2 (Ser217/221; 41G9, #9154), β-tubulin (9F3, #2128) antibodies were from Cell Signaling. GSK3α/β (EP933Y, #2199), p-GSK3α/β (Tyr279/216; ERP933Y, #2309), p-STAT3 (S727; E121-31, #1121) antibodies were from Epitomics. p-GSK3β -S21/S29 (LS-C96880) from Lifespan and β-actin (8226-HRP, ab20272, or ab6276) antibodies from Abcam. Secondary antimouse antibodies were from Roche Diagnostics (HRP-label, #2015216) and Invitrogen (AP-label, WB20006). Secondary antirabbit was purchased from Epitomics (3053-1). Used primary antibodies were validated with recombinant protein, stimulated cell lysates or standards from commercial ELISA kits and selected from a panel of 3 to 5 evaluated antibodies. Compatibility with applied lysis buffer and with antigen concentrations present in analyzed xenografts was checked by a prepared standard MDA-MB-231 tumor lysate. Western blots of total protein were obtained by stripping the phospho-blots and reprobing with the total protein antibody. If not indicated otherwise the loading controls were generated by stripping of the total protein blots and reprobing with β-actin antibody.

Leupeptin, aprotinin, PMSF, and orthovanadate were from Sigma. Glycerol was from Gibco, Triton-X-100 from Roche, Tris buffer pH 8.0 from Roth, and sodium chloride from Merck Darmstadt.

Xenograft studies

Immunodeficient SCID/bg mice were purchased from Charles River (Sulzfeld). Animals used in experiments were between 8 and 16 weeks of age. All experiments were conducted in accordance with local governmental regulations (Regierung von Oberbayern) and Roche internal guidelines. *In vitro* passage numbers 4 and 5 were used for inoculation. A total of 1×10^7 for MDA-MB-231 and 5×10^6 for PL-45, respectively, were injected subcutaneously into the right flank of mice. RG7356 was administered intraperitoneally in once-weekly intervals at the indicated doses. Control animals received vehicle (20 mmol/L histidine, 150 mmol/L NaCl, 0.01% Tween 80). Tumor volume (TV) was measured and calculated according to the NCI protocol [$TV = (\text{length} \times \text{width}^2)/2$], where length and width are long and short diameters of tumor mass in millimeters (13). At necropsy, tumors were excised and immediately shock frozen in liquid nitrogen.

Generation of Cy5-labeled antibody

The purified mAb RG7356 was incubated in 100 mmol/L potassium phosphate, pH 8.5 in a molar ratio of 1:5 with Cy5 NHS ester (GE #PA15101) dissolved in DMSO. The reaction was stopped after 60 minutes by addition of L-lysine up to 10 mmol/L and the surplus of the labeling reagent was removed by dialysis against 20 mmol/L histidine, 200 mmol/L sodium chloride, 5% Saccharose, pH 6.0. The labeling degree was determined using the absorbance of 280 and 650 nm (see product booklet NHS Esters; http://www.gelifesciences.com). The integration ratio of dye to antibody for the present Cy5-labeled antibody was 3:1. Similar binding properties of the parental and Cy5-labeled RG7356 were confirmed by BIACORE analysis (data not shown).

Optical imaging

Near infrared fluorescence imaging was carried out to evaluate tumor penetration and accumulation of the Cy5-labeled RG7356 and to check for its binding properties in histologic sections.

Female SCID beige mice carrying either MDA-MB-231 or PL-45 tumors of about 150 mm^3 were injected via the tail vein with 50 μg Cy5-labeled antibody per animal, which corresponds to a dosage of approximately 2 mg/kg. Mice were sacrificed 24 hours after the administration, tumors were collected and processed histologically to enable *ex vivo* optical fluorescence imaging in histologic sections by using the NUANCE detection system.

Preparation of tumor lysates for Western blot and ELISA

Excised and weighed tumors were mechanically homogenized in liquid nitrogen using mortar and pestle. After homogenization and before thawing of the powdered tissue tumor lysis buffer (1,000 μL per 100 mg of tumor tissue, composition: 10 mmol/L Tris buffer at pH 8.0, 137 mmol/L NaCl, 1% Triton X-100, 10% glycerol, 10 μg/mmol/L aprotinin, 10 μg/mL leupeptin, 1 mmol/L PMSF, 0.4 mmol/L orthovanadate) was added. The material was carefully mixed and transferred to Eppendorf tubes and allowed to thaw completely for 15 minutes at 4°C. Subsequently the lysate was centrifuged for 15 minutes at 20,000 × *g* and 4°C. After removal of the fat layer the supernatant was separated from the solid pellet material, split in aliquots and stored at −80°C until analysis. An aliquot was assessed by BCA-assay (Thermo Scientific #23223) giving protein concentrations in the range of 5 to 10 mg/mL. Typical loading used for gels was 20 μg per lane (10–12 lane gels) or 10 μg per lane for 24 lane gels.

Preparation of tumor lysates and enrichment of phosphopeptides

Excised and weighed tumors were diluted in 1 mL ice cold 8 M urea lysis buffer (see above)and the tissue was homogenized by using an ultraturrax disperser and sonication. Cell debris was sedimented by centrifugation. Protein concentrations were determined by Bradford and to each xenograft sample the same protein amount of the SILAC-labeled MDA-MB-231 reference cell lysate was added. After reduction (5 mmol/L dithiothreitol, 30 minutes 37°C) and alkylation (22 mmol/L iodoacetamide, 30 minutes at room temperature) of cysteine residues the proteins were digested by the addition of lysyl enpopeptidase for 4 hours (Wako; 1:300, w/w). After dilution to about 2 M urea with 20 mmol/L Tris pH 8.2 digestions

Published OnlineFirst July 9, 2012; DOI: 10.1158/0008-5472.CAN-12-0136

were further carried out after the addition of trypsin (Promega; 1:100, w/w) over night. The peptide mixtures were acidified by addition of TFA to a final concentration of 0.5% and subsequently desalted via C18 Sep-Pak columns (Waters) as described by the manufacturer. Peptides were eluted with 50% acetonitrile, 0.5% acetic acid, frozen in liquid nitrogen, lyophilized and subjected to strong cation exchange (SCX) chromatography to prefractionate the crude peptide sample based on a previously described protocol (14) using a PolySULFOETHYL A column (PolyLC; 150 × 4.6 mm, 200 Å pore size and 5 mm particle size) operated with an Äkta Explorer system (GE Healthcare). Briefly, the dried peptides were reconstituted in 1 mL SCX buffer A (5 mmol/L K_2HPO_4, pH 2.7, 30% acetonitrile) and loaded onto the SCX column. The peptides were then separated by a linear gradient from 0% to 25% SCX buffer B (buffer A supplemented with 500 mmol/L KCl) over 32 minutes at a flow rate of 1 mL/min Fractions of 1.5 mL were collected across the gradient and combined to 12 distinct samples. These samples were then lyophilized and the dried peptides were subsequently reconstituted in 1 mL of 0.1% TFA and desalted by using C18 reversed phase cartridges (Waters) as previously described and lyophilized again. Phosphopeptides of each sample were reconstituted in IMAC binding buffer (40% acetonitrile, 25 mmol/L formic acid) and phosphopeptides were enriched by means of PHOS-Select iron affinity beads (Sigma) based on the protocol by Villen and colleagues (14). Briefly, 5 μL of equilibrated IMAC beads were loaded onto in-house made IMAC-C18-STAGE-Tips (IMAC-StageTips) and the peptide samples were loaded by centrifugation (3,000 rpm). The flow-through was collected and repeatedly loaded onto a second IMAC-StageTip. After washing with 1% formic acid, the phosphopeptides were eluted onto the C18 material frit with 500 mmol/L K_2HPO_4. Phosphopeptides were eluted with 50% acetonitrile, 0.5% acetic acid, after additional washing steps with 1% and 0.5% acetic acid, and dried in a vacuum concentrator (Eppendorf) and reconstituted in 0.5% acetic acid before MS-analysis.

ELISA

The commercial p-ERK1/2 Duoset from R&D Systems (DYC185) was chosen for background and sensitivity optimization with alternative blocking buffers. Because the original ELISA was not sensitive enough to measure the p-ERK concentrations present in MDA-MB 231 lysates, the blocking buffer and Diluent #1 were replaced by CrossDown buffer (A6485) from AppliChem Darmstadt to reduce unspecific binding. See Supplementary Fig. S4 for details. p-STAT3 (S727)-ELISA was obtained from cell signaling and used according to the manufacturer's manual. Samples were measured as duplicates either 100 μg (orientating acute study) or 200 μg (time-course acute study) each.

Statistical analysis (Western blot and ELISA)

Developed films were scanned by Image Scanner III (GE Healthcare) and pixel density of spots quantified by ImageQuant 7.0 (GE Healthcare). Statistical significance was checked by using the double side Student *t* test.

Mass spectrometric analysis

The peptide samples were directly loaded onto a self-made reversed phase analytical column (Reprusil-Pur C18-AQ, 3 μm, Dr Maisch GmbH) at a flow rate of 500 nL/min and eluted at a flow rate of 200 nL/min over a gradient from 2% to 30% acetonitrile into an Orbitrap XL mass spectrometer using an Agilent 1,200 nanoflow chromatography system. The Orbitrap mass spectrometer was operated in a data-dependent acquisition mode cycling between full scans in the Orbitrap mass analyzer at a resolution 60,000 and a target value of 1,000,000 charges and the acquisition of 5 consecutive fragmentation spectra (MS/MS mode) of the most abundant peptide ions in the linear ion trap at a target value of 5,000 charges. Ions that were once selected for data-dependent acquisition were 30 seconds dynamically excluded for further fragmentation. To achieve maximal mass accuracy for survey scans, the lock-mass option was enabled. Moreover, for optimal phosphopeptide dissociation the multistage activation modus was enabled in the MS/MS mode.

Mass spectra were processed using the MaxQuant software package (version 1.0.13.13, 15, 16), applying the Mascot search engine (version 2.2.0) for peptide and protein identification. A concatenated forward and reversed Uniprot database (version: 57.12) was used. Regarding the search parameters, the minimal peptide length was set to 6 amino acids, trypsin was selected as proteolytic enzyme and a maximum of 3 missed cleavage sites were allowed. Carbamidomethylation of cysteines was selected as fixed modification, whereas methionine oxidation, N-terminal protein acetylation and phosphorylation of serine, threonine and tyrosine residues were considered as variable modifications. As MaxQuant automatically extracts isotopic SILAC peptide pairs the corresponding isotopic forms of lysine and arginine were automatically selected. The maximal mass deviations of precursor and fragment ion masses were set to 7 ppm and 0.5 Da, respectively. A false discovery rate (FDR) of 0.01 was selected for proteins and peptides and a posterior error probability below or equal to 0.1 for each peptide-to-spectral match was required.

MaxQuant postprocessing

The quantitative information on the phosphorylated sites returned by MaxQuant was further processed as described in (17). In brief, the contaminants, the reverse hits, and the non-class I sites (18) were removed, the ratios between treated samples and vehicle controls were calculated, and the ratios were $\log_{10}$-transformed.

Hierarchical clustering

To get an overview of the regulation occurring in the 3 different time points, hierarchical clustering analysis was applied. First, the means over each experiment's 3 replicates were computed, and sites with mean values in all of the 4 experiments (3 time points plus vehicle control) were subjected to the clustering. The hierarchical clustering was carried out with SpotFire (Tibco) using Ward's method with Euclidean distance as similarity measure.

Published OnlineFirst July 9, 2012; DOI: 10.1158/0008-5472.CAN-12-0136

Significance analysis

The global rank test (19) is applied to find significantly regulated phospho-sites. The original algorithm was not designed to handle missing data, thus we split the dataset into 2 subsets, one containing only sites with all 3 ratios present and one containing those with one missing value. For a fixed FDR level of 0.05 (estimated nonparametrically as described in ref. 19), the size of the top and bottom lists (i.e., top-T and bottom-T, respectively) were then determined independently for sites with 3 ratios and sites with 2 ratios.

Functional enrichment analysis

Functional enrichment analysis was carried out using Ingenuity Pathway analysis (Ingenuity Systems, http://www.ingenuity.com/). Phosphorylation sites identified using the global rank test were associated with biological functions and canonical pathways in Ingenuity's Knowledge Base. A right-tailed Fisher's exact test was used to calculate a *P*-value determining the probability that each biologic function or canonical pathway assigned to the data is because of chance alone.

z-Score calculation

z-Scores were calculated for each phosphorylation site based on the phosphosite's mean ratio and a globally estimated standard deviation (20). In addition, a 2-sided *P*-value was computed for each *z*-score, which was used for the in-depth analysis of enriched pathways. Correction for multiple hypothesis testing was not necessary, because the pathway had been identified as significantly enriched beforehand.

Subnetwork detection

The SubExtractor algorithm aims for extracting significantly regulated subnetworks from STRING. The program is described in detail in ref. 20. In brief, SubExtractor combines phosphoproteomic data with protein–protein interaction data via a Bayesian probabilistic model. Significantly regulated subnetworks are found with a genetic algorithm and subsequent significance evaluation based on the global rank test. The STRING database used for subnetwork extraction was preprocessed to contain only human interactions with a confidence score >0.9. The algorithm's parameters were set to $\alpha = 1.0$ and $\widehat{\sigma} = 5.0$, and subnetworks with an FDR < 0.05 were reported.

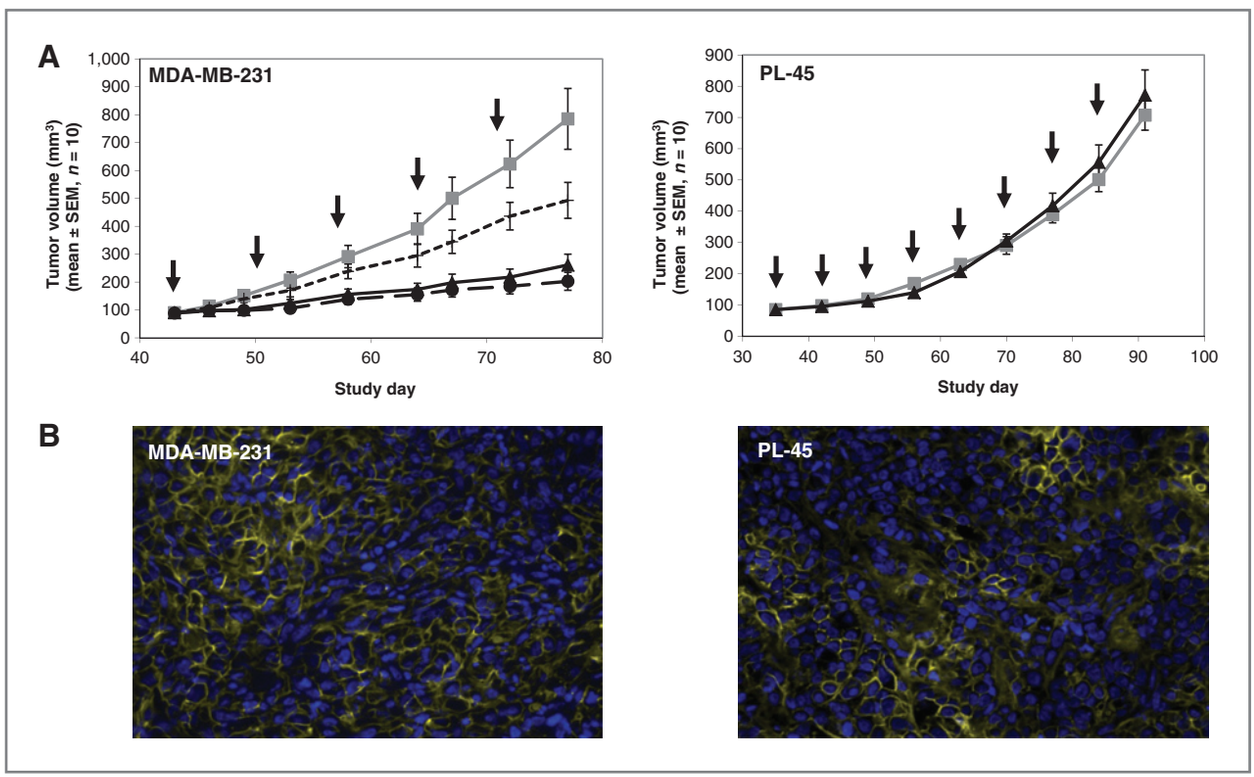

Figure 1. Dose-dependent antitumor efficacy of RG7356 in subcutaneous human xenograft models in female SCID/bg mice. A, established MDA-MB-231 breast adenocarcinoma tumors (90 mm^3; $n = 10$ mice per group) were treated every 7 days, 5 times, intraperitoneally with RG7356. Compared with vehicle control (gray line), RG7356 treatment resulted in a dose-dependent inhibition of tumor growth of 52% for 0.1 mg/kg (dotted black line), 85% for 1 mg/kg (dashed black line), and 81% for 10 mg/kg (solid black line); $P < 0.05$. Established PL-45 pancreatic adenocarcinoma tumors (85 mm^3; $n = 10$ mice per group) were treated every 7 days, 8 times, intravenously with RG7356. Compared with vehicle control (gray line), RG7356 treatment with 30 mg/kg (solid black line) did not show any inhibition of tumor growth. Data in the graphs are mean ± SEM. Arrows indicate the treatment time points. B, binding of Cy5-labeled RG7356 in representative histologic sections of MDA-MB-231 or PL-45 xenografts. Tumor sections were prepared 24 hours after a single intravenous administration of 50 μg Cy5-labeled RG7356 per animal. Distinct Cy5 signals were detected at the marginal area of tumor cells indicating similar membrane localization of the labeled antibody in MDA-MB-231 as well as in PL-45 xenografts. Four hundred fold magnification; nuclei are depicted in blue; Cy5-labeled RG7356 is depicted in yellow.

Published OnlineFirst July 9, 2012; DOI: 10.1158/0008-5472.CAN-12-0136

Results

Xenograft results

RG7356 was shown to significantly inhibit tumor growth in a panel of xenograft models from breast, pancreas, liver, and hematologic origins (21, 22). Weekly doses as low as 1 mg/kg, produce >80% tumor growth inhibition as shown exemplarily for the HER2-negative breast cancer cell line MDA-MB-231 (Fig. 1A). However, not all CD44-expressing cells respond to RG7356 treatment: *in vivo* tumor growth of pancreatic cancer cell line PL45 is unaltered under RG7356 therapy up to 30 mg/kg weekly dosing, despite having similar CD44 surface levels as MDA-MB-231 (FACS analysis *in vitro* and IHC at start and end of treatment period, data not shown) and a similar tumor binding and penetration pattern as shown by *in vivo* imaging experiments using Cy5-labeled RG7356 (Fig. 1B).

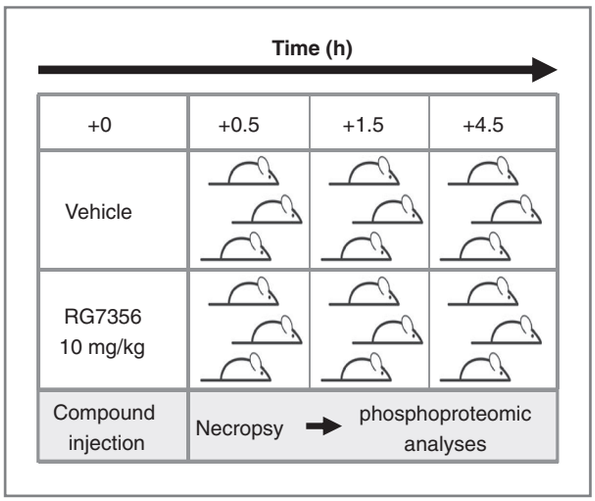

Figure 2. *In vivo* time-course for phosphoproteomic analysis of short-term effects of RG7356 on established MDA-MB-231 breast adenocarcinoma subcutaneous human xenograft in female SCID/bg mice. Tumor-bearing mice (tumor volume 220–240 mm^3; $n = 3$ mice per group and time-point) were treated once with either vehicle or 10 mg/kg of RG7356 at the beginning (+0 hours). At the time points indicated, 3 mice from each therapy group were sacrificed. Tumors were excised and lysates prepared for phospoproteomic analyses (+0, +0.5, +1.5, and +4.5 hours, respectively).

Phosphoproteomic analysis

Understanding the factors that predict response to targeted therapies (response prediction marker), as well as having an early marker of treatment success (pharmacodynamic marker) are mandatory prerequisites for clinical development of (targeted) anticancer compounds. Whole genome profiling is mostly used for biomarker discovery. However, systematic analysis of gene expression profiles needs to be independently confirmed because of a general lack of correlation between transcript and protein levels (23). The proteome/phosphoproteome is closest to function, because it is the proteins that perform most of the chemical reactions necessary for the cell (24). Recent advantages in mass spectrometry–based phosphoproteomics allow monitoring the phosphorylation events in a global, unbiased, and quantitative manner (17, 18, 25, 26). These methods are applied here to analyze the effects of anti-CD44 treatment on MDA-MB-231 xenograft tumors. To avoid detection of secondary effects from the mouse tissue microenvironment or the necrotic tumor remainders at the end of a multiple-dose treatment period, we focused our analysis on the detection of the acute, direct effects of a single treatment of tumor-bearing animals with RG7356 or vehicle control followed by tumor excision and *ex vivo* analysis at the time points indicated (+0, +0.5, +1.5, and +4.5 hours respectively; Fig. 2). Furthermore, this minimizes the effect on protein expression, so that a detected change of abundance of phosphorylated

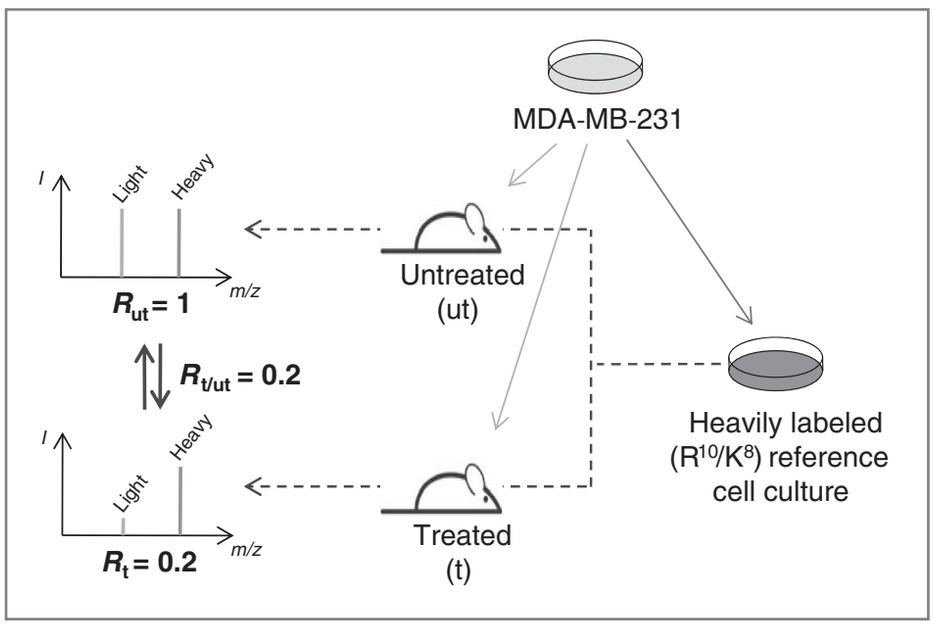

Figure 3. Preparation of Super SILAC reference cell culture for quantitative phosphoproteomics workflow. MDA-MB-231 cells were isotopically labeled with heavy forms of arginine and lysine. The SILAC-labeled reference served as a spike-in for all analyzed xenograft samples to enable a quantitative comparison of the identified protein phosphorylations by mass spectrometry.

Published OnlineFirst July 9, 2012; DOI: 10.1158/0008-5472.CAN-12-0136

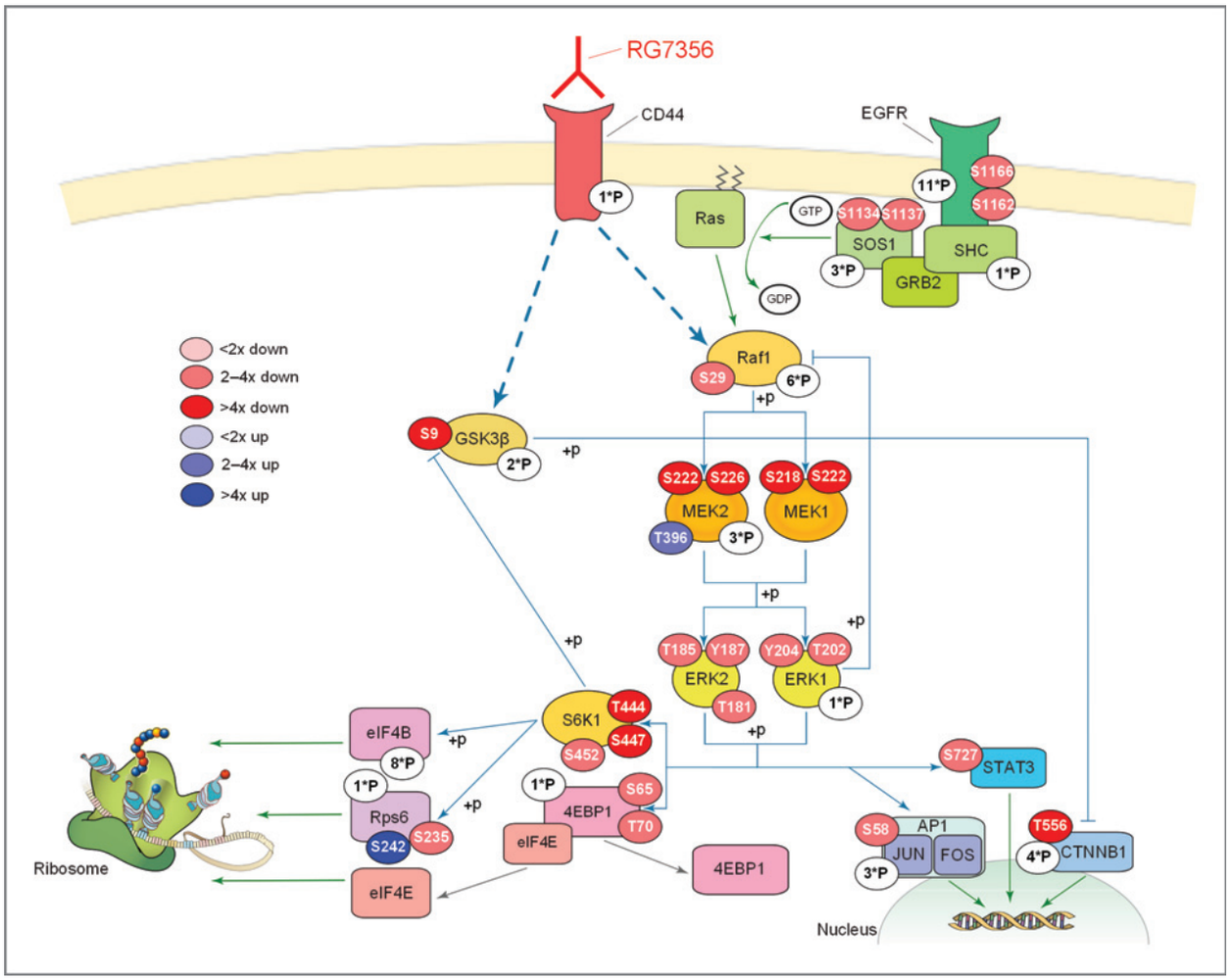

Figure 4. Phosphorylation site–specific pathway analysis focusing on the MAP kinase and downstream signaling pathways for +4.5 hours time point RG7356 treatment versus vehicle control. Red bubbles are downregulated phosphosites, blue bubbles upregulated ones, and white bubbles contain the number of detected but nonregulated sites ($P > 0.05$).

peptides can be deduced to quantitative changes of phosphorylation at the corresponding site.

To quantitatively compare treated versus untreated tumors, the recently published spike-in SILAC technology (27, 28) was adapted for this study (Fig. 3). MDA-MB-231 cells were SILAC labeled with isotopic forms of arginine and lysine *in vitro*. This SILAC standard was then spiked into all xenograft samples, thus enabling a quantitative comparison of the identified phosphorylation sites across the analyzed time points.

For biologic interpretation of the derived mass spectrometric data we only referred to those phosphopeptide hits where the phosphorylation site could be identified with high localization confidence (class-1 sites). Applying the described phosphoproteomics workflow on the mouse xenograft models we were able to quantify 12,669 phosphorylation sites on approximately 3,400 proteins from at least 1 treatment time point against the vehicle control. Overall, 8,820 phosphorylation sites could be quantified in all treatment time points against the vehicle (Supplementary Table S1). On average, about 4 sites per protein were detected with the majority being phosphorylations on serine residues (10,755) followed by threonine (1,707) and tyrosine (207).

Bioinformatics analysis

Hierarchical clustering of all phosphorylation sites detected and quantified in all 3 time points showed that the phosphoproteome is most severely impacted at the latest time point measured (+ 4.5 hours). Overall 381 significantly regulated phosphorylation sites were observed by the global rank test (325 with ratios >2); 134 were downregulated and 247 were found to be upregulated upon treatment.

In addition, all 8,820 quantified class-1 sites were used as input for the SubExtractor algorithm (20), which detects significantly regulated subnetworks in STRING. The main idea of this tool is to combine local as well as topological information, that is, information about the regulation of a certain node (represented by the protein's strongest regulated phosphorylation site) and information about the connectivity with its

Published OnlineFirst July 9, 2012; DOI: 10.1158/0008-5472.CAN-12-0136

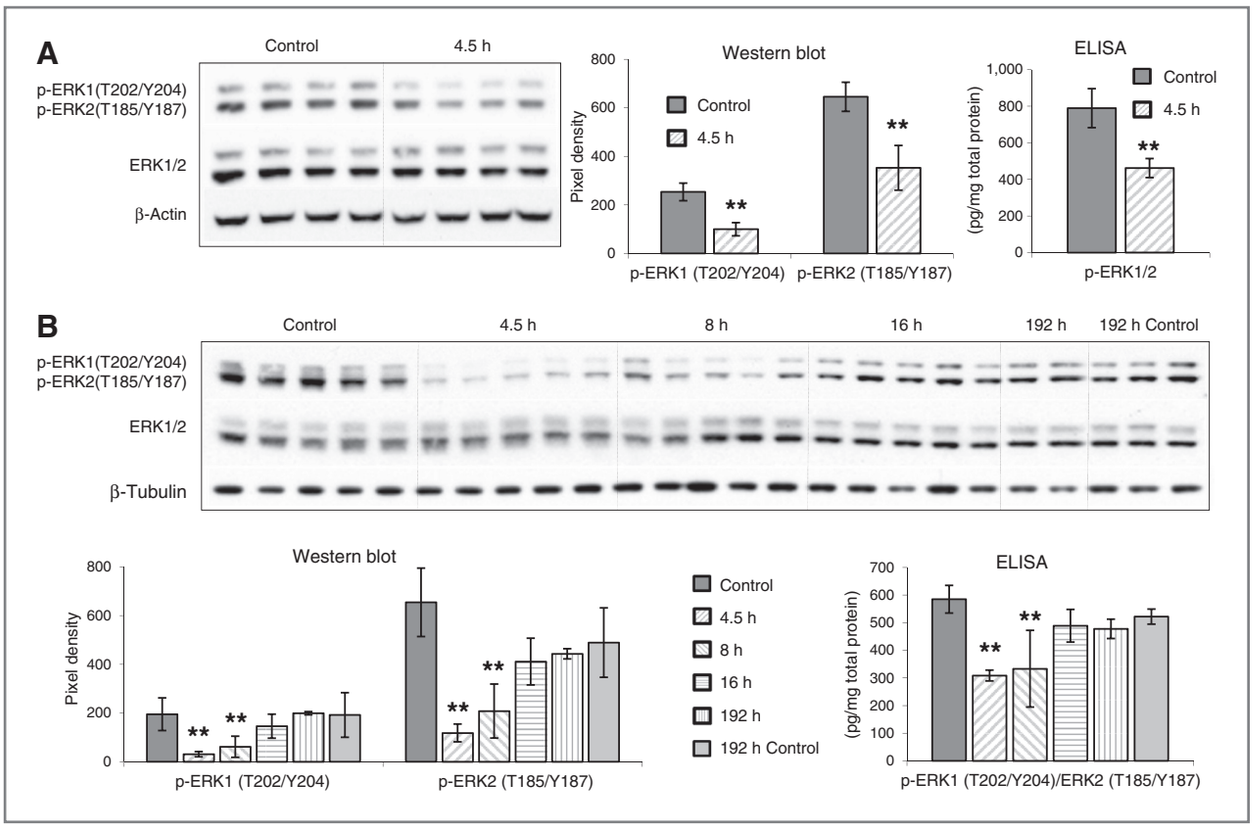

Figure 5. Downmodulation of p-ERK-signaling by RG7356 in MDA-MB-231 xenografts. A, orientating acute study; p-ERK (T202/Y204) signal of vehicle control versus RG7356 treatment at +4.5 hours (p-ERK1, p-ERK2, $P < 0.001$, double side t test). Duplicates of 100 μg protein were used for ELISA, $P < 0.01$. B, time-course acute study: p-ERK (T202/Y204) signal of vehicle controls versus RG7356 treatment at +4.5, +8, +16, and +192 hours, respectively ($P < 0.01$ for +4.5 and +8 hours). A separate β-tubulin blot was used as loading control. ELISA: duplicates of 200 μg each ($P < 0.001$ for +4.5 and $P < 0.01$ for +8 hours).

neighbors. The probability of a node to be a member of a regulated subnetwork increases the stronger a node is regulated and the more interactions it has to well-regulated neighbors.

The largest subnetwork that has been identified by SubExtractor (FDR level 0.05) centered around the MAPK cascade and comprises different biologic processes such as transcription and translation, the architecture of the nuclear core complex, but also cell-cycle regulation and signal transduction (Supplementary Fig. S1). The latter included Rho GTPase-mediated signaling, which is involved in cell morphology and adhesion/migration control. Similarly, when using the same dataset in a functional enrichment analysis using Ingenuity Pathway Analysis (Ingenuity Systems, http://www.ingenuity.com/), the biologic functions significantly affected by RG7356 treatment were mainly associated with processes and features like cell-cycle progression, cell morphology and cellular development all of which are regulated by the MAPK pathway (data not shown).

Enrichment analysis of the significantly regulated phosphorylation sites with respect to canonical pathways again using Ingenuity Pathway Analysis similarly identified the MAPK/ERK signaling cascade at the center of proteins affected by RG7356 treatment. In-depth analysis on the level of regulated individual phosphorylation sites within the MAP kinase pathway based on the z-score P-values (Fig. 4) showed regulated serine phosphorylation sites on the EGF receptor and the associated adaptor protein Sos1. Furthermore, highly regulated sites were found on members of the Raf/MEK/ERK cascade. Notably, the regulated sites found here were direct targets of the preceding upstream kinases (S218/S222 and S222/S226 on MEK1 and MEK2, respectively; Y204/T202 and Y187/T185 on ERK1 and ERK2, respectively). Despite the fact that tyrosine phosphorylations were in principle accessible with the phosphoproteomics technology applied in this study (207 tyrosine phosphorylations identified), no tyrosine phosphorylations were monitored on EGFR.

The downregulation of phosphorylation sites was further transmitted to the ribosomal protein S6 kinase 1 (29–31) and the translation initiation factor binding protein 4EBP1 (32, 33). Both proteins play key roles in the initiation of ribosomal protein translation and 4EBP1 phosphorylation is responsible for the release of the translation initiation factor eIF4E. The corresponding functional site on 4EBP1 (T70) was found to be downregulated, which leads to a stabilization of the protein complex and consequently to a suppression of protein translation.

Published OnlineFirst July 9, 2012; DOI: 10.1158/0008-5472.CAN-12-0136

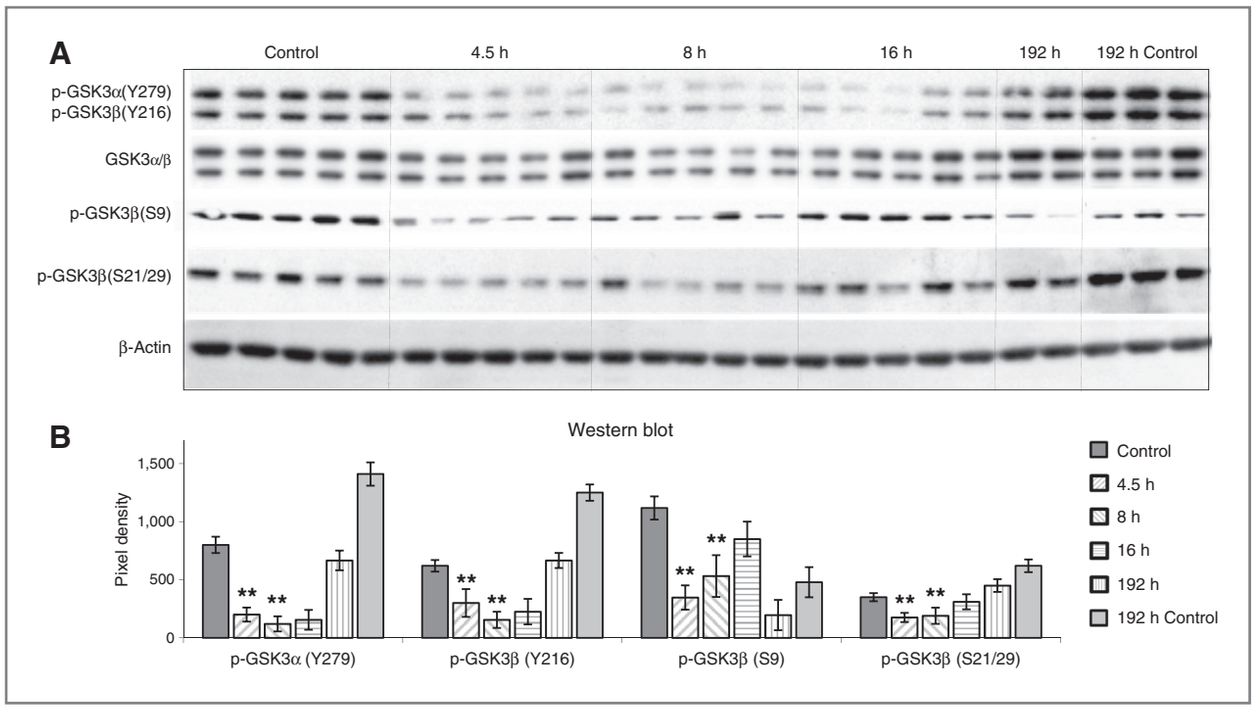

Figure 6. Downmodulation of GSK3-signaling by RG7356 in MDA-MB-231 xenografts. A, p-GSKα/β-Y279/216 signal of vehicle control versus RG7356 treatment at +4.5, +8, +16, and +192 hours, respectively; p-GSKβ (S9) signal of vehicle control versus RG7356 treatment at +4.5, +8, +16, and +192 hours, respectively. p-GSKβ (S21/S29) signal of vehicle control versus RG7356 treatment at +4.5, +8, +16, and +192 hours, respectively. Western blot was washed and reprobed with β-actin antibody and detected by an antimouse-AP antibody. B, digitalized Western blots; downmodulation was significant ($P < 0.001$) at +4.5, +8, and +16 hours, respectively, for pY279 (GSK3α) and pY216 (GSK3β), for pS9 (GSK3β) at +4.5 hours ($P < 0.001$), +8 hours ($P = 0.001$), and for S21/S29 (GSK3β) at +4.5 hours ($P < 0.001$).

An effect on transcriptional control can be inferred from the observed downregulation of phosphorylation sites on the transcription factors Jun, CTNB1 and STAT3 (S727).

Confirmation of phosphoproteomics results

Despite its proven reliability to detect even minute alterations of the phosphoproteome under the influence of pharmacological inhibitors (34), we wanted to confirm and extend findings from this high throughput analysis by alternative methodologies. In a first orientating acute study (study design in analogy to Fig. 2, but using 4 animals/group/time point), with tumor lysates from the very same +4.5 hours time point as described earlier, phosphorylation status of p-ERK1/2, p-MEK1/2, p-eIF4E, p-STAT3, and p-GSK3α/β, respectively, was evaluated by Western blot and ELISA assays. Analysis of a second time-course acute study (study design in analogy to Fig. 2, but using 5 animals/group/time point; tumors excised at +0, +4.5, +8, +16, and +192 hours, respectively) by Western blot and ELISA provided further insights on RG7356′s direct effects on tumors *in vivo*.

p-ERK1/2, a pivotal switch of MAPK-pathway signaling and found to be changed in the phosphoproteomics study, was analyzed by Western blot. In a first orientating acute study, a significant downmodulation of the dual phosphorylation site was seen at +4.5 hours. A second time-course acute study confirmed these results and showed significant p-ERK1/2 downmodulation for the +4.5 and +8 hours time points (Fig. 5). Data obtained from an optimized p-ERK ELISA matched the Western blot results and showed significant p-ERK downmodulation for the same time points in both acute studies.

There was high variance in p-MEK as an upstream signal of p-ERK. With no p-MEK downmodulation seen in the orientating acute study there was in contrast a clear down-modulation of p-MEK after +4.5 hours in the time-course acute study (Supplementary Fig. S2). ERK1/2 is known to associate with GSK3β and prime it for further phosphorylation. p90RSK, a downstream kinase of ERK, is responsible for the phosphorylation of GSK3β at Ser9 (35). This is consistent with the significant reduction of phosphorylation at the Ser9-site of GSK3β that was seen +4.5 and +8 hours after application of RG7356 (Fig. 6). At the same time points and after +16 hours, there was a pronounced downmodulation ($P < 0.001$) of the activating phosphorylation sites Tyr216 (36) in GSK3β as well as Tyr279 in GSK3α during the time-course acute study. For these 2 activating tyrosine-sites, there is a significant enhancement of the phosphosignal after 192 hours compared with the 4.5 hours control. We interpret this as an adaption to metabolic changes that are triggered by increased hypoxia and accelerated tumor growth. Despite this increased phosphorylation in the untreated group, RG7356 shows a long-lasting reduction of GSK3α (Y279) and GSK3β (Y216) phosphorylation even at 192 hours. These results suggest that the induction of downstream metabolic events play a critical role for the response to RG7356. Phosphorylation of the rare double phosphorylation site Ser21/Ser29 present in GSK3β was reduced at +4.5 hours. However,

Published OnlineFirst July 9, 2012; DOI: 10.1158/0008-5472.CAN-12-0136

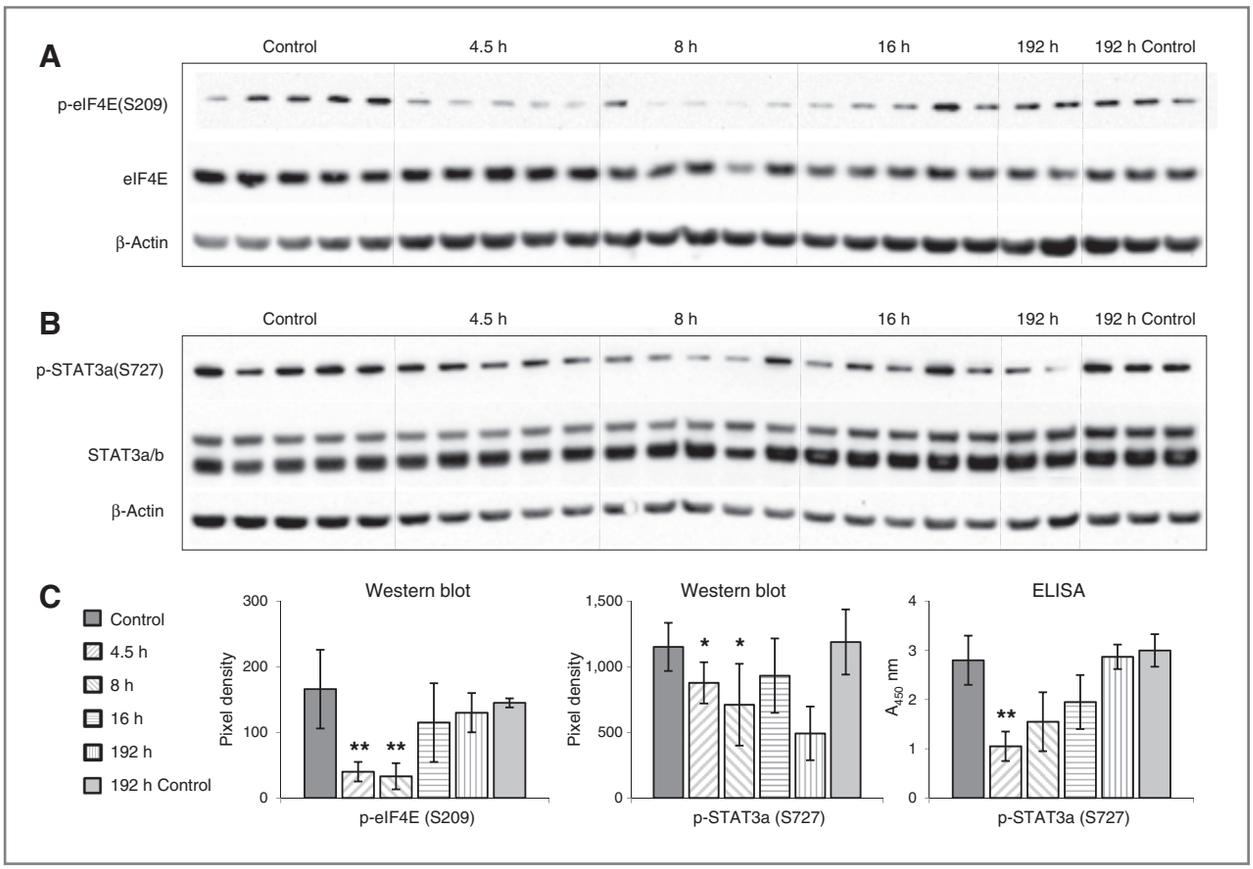

Figure 7. Downmodulation of p-eIF4E and p-STAT3 signaling by RG7356 in MDA-MB-231 xenografts. A, p-eIF4E (S209) signal of vehicle controls versus RG7356 treatment at +4.5, +8, +16, and +192 hours, respectively. B, p-STAT3 (S727) signal of vehicle controls versus RG7356 treatment at +4.5, +8, +16, and +192 hours, respectively. C, digitalized Western blots and p-STAT3-ELISA. Significant downmodulation of p-eIF4E (S209) at +4.5 hours ($P < 0.01$, double-sided *t* test) and +8 hours ($P = 0.01$). Downmodulation of p-STAT3 (S727) at +4.5 and +8 hours ($P < 0.05$) was further confirmed by a p-STAT3 (S727) ELISA, at +4.5 hours ($P < 0.01$).

the biologic relevance of this specific dual phosphorylation site and its downmodulation remains unclear.

Signal transducer and activator of transcription 3 (STAT3), suppressed in normal cells but upregulated or constitutively active in many cancer tissues (37), is an important antiapoptotic transcription factor (38). ERK1/2 is believed to modulate STAT3 activity through phosphorylation at Ser727 (39, 40). The tumor suppression caused by sorafenib has been linked at least in part to the dephosphorylation of STAT3 induced by inhibition of the MEK/ERK-pathway (41). Our results showed a reduction in p-STAT3 (Ser727) induced by RG7356 after +4.5 and +8 hours (Fig. 7), a finding also confirmed by a corresponding ELISA.

Eukaryotic initiation factors (eIF4s) are important regulators of protein synthesis and selective translation of specific mRNAs that promote human cancer development (42). Stimulation of ERK and p38 MAPK has been shown to trigger phosphorylation of eIF4 at Ser209 (43, 44). Changes in eIF4E-levels affect translation rates of proteins related to cell growth and survival involved in oncogenesis, for example, c-Myc, cyclin D1, and Mcl-1 (45). Therefore, inhibition of eIF4E effectively suppresses cellular transformation and tumor growth. Consistently, treatment by RG7356 caused a significant reduction of eIF4E activation at Ser209 after 4.5 and 8 hours ($P \leq 0.01$).

Effect on MAPK pathway in nonresponder cell line

Western blot analysis of tumor lysates from a PL45 acute study (study design in analogy to Fig. 2), a tumor that did not respond to anti-CD44 therapy as exemplified in Fig. 1, did not show any alteration of MAPK and related phosphorylation events as observed for MDA-MB-231 tumors (Supplementary Fig. S3).

Discussion

The crucial role of the adhesion receptor CD44 in tumor cell behavior is well documented in the literature. CD44 is involved in survival, progression, and metastasis of cancer and numerous reports describe the role of CD44 in cell–cell and cell–matrix interactions with various partners as well as the function of CD44 to act as a sensor for changes in the tumor microenvironment. However, despite this broad experimental evidence, it is still unclear how pharmacological targeting of CD44 exerts its effects on tumor cells (46). Rather, the current

Published OnlineFirst July 9, 2012; DOI: 10.1158/0008-5472.CAN-12-0136

knowledge on CD44 biology consists of a compendium of individual results that do not always fit together and are mostly based on *in vitro*, rather than *in vivo* results. This situation is further complicated by the structure of CD44 itself, which can be modified by *N*- and *O*-glycosylation as well as alternative splicing, producing potentially hundreds of CD44 variants described of having differing roles in diseased and healthy tissues. Herein, we describe a novel approach to determine the direct effect of targeting CD44 with a humanized monoclonal antibody, RG7356, by global quantitative phosphoproteomics analysis of freshly isolated xenograft tumors. This approach has several advantages compared with other high- or medium-throughput methodologies such as gene-expression profiling or pull-down assays on immobilized proteins followed by mass-spectrometry (47): (i) unbiased -omics approach that provides information on whole pathways rather than single events, (ii) quantitative, (iii) applicable for *in vitro* and *in vivo* studies, (iv) captures the direct effect of treatment on phosphorylation events, (v) can be correlated to *in vivo* efficacy, and (vi) findings can be easily verified by conventional methodology and translated to other responder/nonresponder models. Although s.c. xenografts do not fully represent the environment that tumors grow in or metastasize to, this setting was chosen to guarantee access to sufficient amounts of tumor material for *ex vivo* analysis and to focus on determining the direct effects of antibody binding to the tumor rather than looking at tumor–stroma interactions or other secondary effects.

RG7356 is a recombinant human antibody of the IgG1-kappa isotype that specifically binds to the constant region of the extracellular domain of the human cell-surface glycoprotein CD44 that is present on CD44 standard as well as on all CD44 splice variants. Immunohistochemistry and FACS analysis reveal that the RG7356 binding epitope is present on a broad panel of cancer cell lines and patient samples from solid tumor and hematologic malignancies. The antibody interferes with CD44 HA interactions but does not seem to influence turnover, downregulation, or shedding of CD44: *ex vivo* analysis of xenograft tumors showed no alteration of CD44 surface expression even after prolonged treatment periods.

Short-term treatment of MDA-MB-231 xenografts, that were previously shown to respond to RG7356 treatment *in vivo*, results in a very rapid (~0.5–8 hours) downmodulation of the phosphorylation of the MAPK pathway. Findings from the global phosphoproteomics approach were independently verified by Western blot and ELISA analyses that completely matched the initial mass spectrometry results. When evaluating the effect of RG7356 acute treatment on the nonresponsive PL45 cell line, no alterations of MAPK or related phosphorylations could be observed. In conclusion, these studies show that CD44 is directly involved in the activation of MAPK pathway regulated growth of tumors that are sensitive to anti-CD44 treatment.

CD44 has been associated with alterations in the MAPK pathway before (48–50). However, this is the first study to show a time-course effect on MAPK pathway caused by the pharmacological inhibition of CD44 rather than indirect methodology such as manipulation of the protein itself at the gene expression level (knockdown or forced expression) or interaction studies with the receptor using hyaluronic acid or fragments thereof.

Findings of this study provide further insights into the potential mode of action of targeting the constant region of CD44 with an antibody, potentially leading to relevant pharmacodynamics and response prediction markers to help guide the preclinical and clinical development of RG7356. Further studies to prove the utility of this methodology as well as the relevance of this finding for RG7356 are warranted.

Disclosure of Potential Conflicts of Interest

No potential conflicts of interest were disclosed.

Authors' Contributions

Conception and design: S. Weigand, F. Herting, A. Nopora, E. Voss
Development of methodology: F. Herting, A. Nopora, E. Voss, A. Tebbe
Acquisition of data (provided animals, acquired and managed patients, provided facilities, etc.): S. Weigand, F. Herting, A. Nopora, E. Voss, A. Tebbe
Analysis and interpretation of data (e.g., statistical analysis, biostatistics, computational analysis): D. Maisel, A. Nopora, E. Voss, C. Schaab, M. Klammer
Writing, review, and/or revision of the manuscript: S. Weigand, F. Herting, D. Maisel, A. Nopora, E. Voss, C. Schaab, M. Klammer, A. Tebbe
Administrative, technical, or material support (i.e., reporting or organizing data, constructing databases): S. Weigand, D. Maisel, A. Tebbe
Study supervision: S. Weigand, A. Tebbe

Grant Support

This study was financed by Roche Diagnostics GmbH, Nonnenwald 2, 82377 Penzberg, Germany.

The costs of publication of this article were defrayed in part by the payment of page charges. This article must therefore be hereby marked *advertisement* in accordance with 18 U.S.C. Section 1734 solely to indicate this fact.

Received January 24, 2012; revised June 5, 2012; accepted June 19, 2012; published OnlineFirst July 9, 2012.

References

1. Gotte M, Yip GW. Heparanase, hyaluronan, and CD44 in cancers: a breast carcinoma perspective. Cancer Res 2006;66:10233–7.
2. Afify A, Purnell P, Nguyen L. Role of CD44s and CD44v6 on human breast cancer cell adhesion, migration, and invasion. Exp Mol Pathol 2009;86:95–100.
3. Louderbough JMV, Schroeder JA. Understanding the dual nature of CD44 in breast cancer progression. Mol. Cancer Res 2011;9: 1573–86.
4. Ringel J, Jesnowski R, Schmidt C, Ringel J, Köhler HJ, Rychly J, et al. CD44 in normal human pancreas and pancreatic carcinoma cell lines. Teratog Carcinog Mutagen 2001;21:97–106.
5. Gotoda T, Matsumura Y, Kondo H, Saitoh D, Shimada Y, Kosuge T, et al. Expression of CD44 variants and its association with survival in pancreatic cancer. Jpn J Cancer Res 1998;89:1033–40.
6. Yang GH, Fan J, Xu Y, Qiu SJ, Yang XR, Shi GM, et al. Osteopontin combined with CD44, a novel prognostic biomarker for patients with hepatocellular carcinoma undergoing curative resection. Oncologist 2008;13:1155–65.
7. Liu J, Jiang G. CD44 and hematological malignancies. Cell Mol Immunol 2006;3:359–65.
8. Zöller M. CD44: can a cancer-initiating cell profit from an abundantly expressed molecule? Nat Rev Cancer 2011;11:254–67.

Published OnlineFirst July 9, 2012; DOI: 10.1158/0008-5472.CAN-12-0136

9. Ponta H, Sherman L, Herrlich PA. CD44: from adhesion molecules to signaling regulators. Nat Rev Mol Cell Biol 2003;4:33–45.
10. Orian-Rousseau V. CD44, a therapeutic target for metastasizing tumors. Eur J Cancer 2010;46:1271–7.
11. Toole BP, Ghatak S, Misra S. Hyaluronan oligosaccharides as a potential anticancer therapeutic. Curr Pharm Biotechnol 2008;9:249–52.
12. Robertson BW, Bonsal L, Chellaiah MA. Regulation of Erk1/2 activation by osteopontin in PC3 human prostate cancer cells. Mol Cancer 2010;9:260.
13. Corbett TH, Valeriote FA, Demchik L, Lowichik N, Polin L, Panchapor C, et al. Discovery of cryptophycin-1 and BCN-183577: examples of strategies and problems in the detection of antitumor activity in mice. Invest New Drugs 1997;15:207–18.
14. Villen J, Gygi P. The SCX/IMAC enrichment approach for global phosphorylation analysis by mass spectrometry. Nat Protoc 2008;3: 1630–8.
15. Cox J, Mann M. MaxQuant enables high peptide identification rates, individualized p.p.b.-range mass accuracies and proteome-wide protein quantification.Nat Biotechnol 2008;26:1367–72.
16. Cox J, Matic I, Hilger M, Nagaraj N, Selbach M, Olsen JV, et al. A practical guide to the MaxQuant computational platform for SILAC-based quantitative proteomics. Nat. Protoc 2009;4:698–705.
17. Schaab C. Analysis of phosphoproteomics data. Methods Mol Biol 2011;696:41–57.
18. Olsen JV, Blagoev B, Gnad F, Macek B, Kumar C, Mortensen P, et al. Global, *in vivo*, and site-specific phosphorylation dynamics in signaling networks. Cell 2006;127:635–48.
19. Zhou Y, Cras-Meneur C, Ohsugi M, Stormo GD, Permutt MA. A global approach to identify differentially expressed genes in cDNA (two-color) microarray experiments. Bioinformatics 2007;23:2073–9.
20. Klammer M, Godl K, Tebbe A, Schaab C. Identifying differentially regulated subnetworks from phosphoproteomic data. BMC Bioinformat 2010;11:1–13.
21. da Cruz L, McConkey F, Feng N, Pereira D, Hahn S, Rubinstein D, et al. Clinical development of huARH460-16-2: a therapeutic antibody targeting the CD44 cancer stem cell antigen on high-incidence adenocarcinomas. J Clin Oncol 2008;26:20 suppl.; abstr. 14581.
22. da Cruz L, McConkey F, Feng N, Pereira D, Hahn S, Rubinstein D, et al. Anti-CD44 antibody, ARH460-16-2, binds to human AML CD34+CD38- cancer stem cells and shows anti-tumor activity in an AML xenograft model. AACR Meeting Abstracts 2008;2008:3976.
23. Chaerkady R, Pandey A. Quantitative proteomics for identification of cancer biomarkers. Proteomics Clin Appl 2007;1:1080–9.
24. Andersen JS, Mann M. Functional genomics by mass spectrometry. FEBS Lett 2000;480:25–31
25. Mann M. Functional and quantitative proteomics using SILAC. Nat Rev Mol Cell Biol 2006;7:952–8.
26. Macek B, Mann M, Olsen JV. Global and site-specific quantitative phosphoproteomics: principles and applications. Ann Rev Pharmacol Toxicol 2009;49:199–221.
27. Geiger T, Wisniewski JR, Cox J, Zanivan S, Kruger M, Ishihama Y, et al. Use of stable isotope labeling by amino acids in cell culture as a spike-in standard in quantitative proteomics. Nat Protocol 2011;6:147–57.
28. Monetti M, Nagaraj N, Sharma K, Mann M. Large-scale phosphosite quantification in tissues by a spike-in SILAC method. Nat Methods 2011;8:655–8.
29. Iijima Y, Laser M, Shiraishi H, Willey CD, Sundaravadivel B, Xu L, et al. c-Raf/MEK/ERK pathway controls protein kinase C-mediated p70S6K activation in adult cardiac muscle cells. J Biol Chem 2002;277: 23065–75.
30. Zhang Y, Dong Z, Nomura M, Zhong S, Chen N, Bode AM, et al. Signal transduction pathways involved in phosphorylation and activation of p70S6K following exposure to UVA irradiation. J Biol Chem 2001; 276:20913–23.
31. Shi Y, Hsu JH, Hu L, Gera J, Lichtenstein A. Signal pathways involved in activation of p70S6K and phosphorylation of 4E-BP1 following exposure of multiple myeloma tumor cells to interleukin-6. J Biol Chem 2002;277:15712–20.
32. Heesom KJ, Gampel A, Mellor H, Denton RM. Cell cycle-dependent phosphorylation of the translational repressor eIF-4E binding protein-1 (4E-BP1). Curr Biol 2001;11:1374–9.
33. Mothe-Satney I, Brunn GJ, McMahon LP, Capaldo CT, Abraham RT, Lawrence JC. Mammalian target of rapamycin-dependent phosphorylation of PHAS-I in four (S/T)P sites detected by phospho-specific antibodies. J Biol Chem 2000;275:33836–43.
34. Pan C, Olsen JV, Daub H, Mann M. Global effects of kinase Inhibitors on signaling networks revealed by quantitative phosphoproteomics. Mol Cell Proteomics 2009:8:2796–808.
35. Hung MC, Ding Q, Xia W, Liu JC, et al. ERK associates with and primes GSK-3β. Mol Cell 2005;19:159–70.
36. Eldar-Finkelmann H. Glycogen synthase 3: an emerging therapeutic target. Trends Mol Med 2002;8:126–32.
37. Garcia R, Jove R. Activation of STAT transcription factors in oncogenic tyrosine signaling. J Biomed Sci 1998;5:79–85.
38. Catlett-Falcone R, Landowski TH, Oshiro MM, Turkson J, Levitzki A, Savino R, et al. Constitutive activation of Stat3 signaling confers resistance to apoptosis in human U266 myeloma cells. Immunity 1999;10:105–15.
39. Tian ZJ, An W. ERK1/2 contributes negative regulation to STAT3 activity in HSS-transfected HepG2 cells. Cell Res 2004;14: 141–7.
40. Chung J, Uchida E, Grammer JC, Blenis J. STAT3 serine phosphorylation by ERK-dependent and -independent pathways negatively modulates its tyrosine phosphorylation. Mol Cell Biol 1997;17: 6508–16.
41. Gu FM, Li QL, Jiang JH, Huang XY, Pan JF, Fan J, et al. Sorafenib inhibits growth and metastasis of hepatocellular carcinoma by blocking STAT3. World J. Gastroenterol 2011;17:3922–32.
42. Sivera D, Formenti S, Schneider R. Translational control in cancer. Nat Rev Cancer 2010;256:254–66.
43. Waskiewicz AJ, Johnson JC, Penn B, Mahalingam M, Kimball SR, Cooper JA. Phosphorylation of the cap-binding protein eukaryotic translation initiation factor 4E by protein kinase Mnk1 *in vivo*. Mol Cell Biol 1999;19:1871–80.
44. Pyronnet S, Imataka H, Gingras AC, Fukunaga R, Hunter T, Sonnenberg N. Human eukaryotic translation initiation factor 4G (eIF4G) recruits Mnk1 to phosphorylate eIF4E. EMBO J 1999;18: 270–9.
45. Li Y, Yue P, Deng X, Ueda T, Fukunaga R, Khuri F, et al. Protein phosphatase 2A negatively regulates eukaryotic initiation factor 4Ephosphorylation and eIF4F assembly through direct dephosphorylation of Mnk and eIF4E. Neoplasia 2010;12:848–55.
46. Naor D, Wallach-Dayan SB, Zahalka MA, Sioniv RV. Involvement of CD44, a molecule with a thousand faces in cancer dissemination. Semin Cancer Biol 2008;18:260–7.
47. Skandalis SS, Kozlova I, Engström U, Hellman U, Heldin P. Proteomic identification of CD44 interacting proteins. IUBMB Life 2010;62:833–40.
48. Zhang LS, Ma HW, Greyner HJ, Zuo W, Mummert ME. Inhibition of cell proliferation by CD44: Akt is inactivated and EGR-1 is down-regulated. Cell Prolif 2010;43:385–95.
49. Lee JL, Wang MJ, Chen JY. Acetylation and activation of STAT-3 mediated by nuclear translocation of CD44. J Cell Biol 2009;185: 949–57.
50. Hatano H, Shigeishi H, Kudo Y, Higashikawa K. Tobiume K, Takata T, Kamata N. RHAMM/ERK interaction induces proliferative activities of cementifying fibroma cells through a mechanism based on the CD44-EGFR.Lab Invest 2011;91:379–91.

Published OnlineFirst July 9, 2012; DOI: 10.1158/0008-5472.CAN-12-0136

Cancer Research
The Journal of Cancer Research (1916–1930) | The American Journal of Cancer (1931–1940)

AACR American Association for Cancer Research

Global Quantitative Phosphoproteome Analysis of Human Tumor Xenografts Treated with a CD44 Antagonist

Stefan Weigand, Frank Herting, Daniela Maisel, et al.

Cancer Res 2012;72:4329-4339. Published OnlineFirst July 9, 2012.